JOURNAL OF GEOPHYSICAL RESEARCH, VOL. 106, NO. D13, PAGES 14,485–14,500, JULY 16, 2001

A new retrieval for cloud liquid water path using a ground-based microwave radiometer and measurements of cloud temperature

James C. Liljegren,[1] Eugene E. Clothiaux,[2] Gerald G. Mace,[3] Seiji Kato,[4] and Xiquan Dong[3]

Abstract. A new method to retrieve cloud liquid water path using 23.8 and 31.4 GHz microwave radiometer brightness temperature measurements is developed. This method does not depend on climatological estimates of either the mean radiating temperature of the atmosphere T_{mr} or the mean cloud liquid water temperature T_{cloud}. Rather, T_{mr} is estimated from surface temperature and relative humidity measurements, while T_{cloud} is estimated using millimeter-wave cloud radar data, together with atmospheric temperature profiles obtained from either radiosonde or rapid update cycle (RUC) model output. Simulations demonstrate that the new retrieval method significantly reduces the biases in the liquid water path estimates that are apparent in a site-specific retrieval based on monthly stratified, local climatology. An analysis of the liquid water path estimates produced by the two retrievals over four case study days illustrates trends and retrieval performances consistent with the model simulations.

1. Introduction

The critical role of clouds in the radiative balance of the Earth is widely recognized, as is the uncertainty in our understanding of cloud-radiation interactions [*Committee on Earth and Environmental Sciences (CEES),* 1990]. The difficulty in adequately capturing the effects of clouds in atmospheric general circulation models (GCMs) due to these uncertainties is also well documented [*Cess et al.,* 1990]. In their overview of the Earth Observing System (EOS), *Wielicki et al.* [1995] reviewed and emphasized the importance of cloud--radiation interactions to the Earth climate system. Among the variables that *Wielicki et al.* [1995] discussed in the context of cloud-radiation interactions and feedback processes, cloud liquid water path (LWP) was identified as one of the most important.

Evaluation of recent treatments of LWP as a prognostic variable in some GCMs [e.g., *Ghan et al.,* 1997] is also of paramount importance. The chief difficulty from a modeling perspective is that the unresolved sub-grid-scale variations in cloud liquid water significantly affect the mean optical and thermodynamic properties within the model grid box. Somehow these variations must be parameterized in terms of other prognostic variables (cloud water, temperature, etc.) in a computationally efficient manner. To date, the general approach for incorporating cloud water sub-grid-scale variability has been to develop a compact description of the variations of LWP that would apply to all clouds of a particular type (e.g., marine stratus) over a range of prognostic variable values. An example of an approach to quantifying the spatial heterogeneity of cloud-related quantities is based on techniques that seek to describe the self-similar scaling, or fractal, nature of clouds [*Cahalan and Joseph,* 1989; *Cahalan et al.,* 1994; *Davis et al.,* 1994].

To develop both a better understanding of cloud-radiation interactions and more accurate cloud parameterizations in GCMs, accurate measurements of LWP must be available. To acquire such measurements, the U.S. Department of Energy Atmospheric Radiation Measurement (ARM) Program [*Stokes and Schwartz,* 1994] has deployed dual-frequency microwave radiometers [*Liljegren,* 1994] at its facilities in the U.S. Southern Great Plains (SGP), the Tropical Western Pacific (TWP), and the North Slope of Alaska (NSA). A site-specific (i.e., restricted to the specific climatology of the location for which it is derived) statistical retrieval [*Westwater,* 1993] was developed for each location to derive LWP and precipitable water vapor (PWV) from mi-

[1]Environmental Research Division, Argonne National Laboratory, Argonne, Illinois.

[2]Department of Meteorology, The Pennsylvania State University, University Park, Pennsylvania.

[3]Department of Meteorology, University of Utah, Salt Lake City, Utah.

[4]Center for Atmospheric Sciences, Hampton University, Hampton, Virginia.

Paper number 2000JD900817.
0148-0227/01/2000JD900817$09.00

crowave brightness temperatures. Although the statistical algorithm permits the retrieval of LWP and PWV from microwave measurements alone, additional measurements are available at the ARM facilities that can be used to improve the accuracy of the retrieved quantities.

In this paper an improved site-independent statistical retrieval technique for LWP is presented. This technique does not depend on climatology and thus may be applied at any measurement location for which ancillary measurements are available for surface pressure, temperature, humidity, and mean cloud liquid water temperature (e.g., measurements from millimeter-wave cloud radar and sounding data). A formulation is also presented which does not require an estimate of mean cloud liquid water temperature; for this case the accuracy of the algorithm is reduced to that of a site-specific statistical retrieval. The current site-specific statistical retrieval and the new site-independent retrieval are evaluated by using simulated radiometer brightness temperature measurements generated with a microwave radiation transfer model. The site-specific and site-independent retrievals are also compared with the results from an iterative physical retrieval by using measurements from four case study days.

2. Methodology

2.1. Theoretical Basis for the New Retrieval

The atmospheric opacity τ at the measured frequencies of 23.8 and 31.4 GHz is due to the sum of a "dry" contribution $\tau_{\rm dry}$ from the far wing of the 60-GHz oxygen band, a contribution $\tau_{\rm vap}$ from the water vapor resonance centered at 22 GHz, and (for cloudy conditions) a contribution $\tau_{\rm liq}$ from liquid water. We define a frequency-dependent, path-averaged mass absorption coefficient for each contributor i as

$$\bar{\kappa}_i = \frac{\int_0^\infty \kappa_i(z)\ \rho_i(z)\ dz}{\int_0^\infty \rho_i(z)\ dz}. \tag{1}$$

Value $\bar{\kappa}_i$ has no explicit dependence on the vertical distribution of contributor i, whether it be water vapor or liquid water. This feature of $\bar{\kappa}_i$, together with the measurement frequencies selected, significantly simplifies the LWP and PWV retrievals, as will be explained later. We also make use of $\tau_i = \int \kappa_i(z)\ \rho_i(z)\ dz$, $V = \int \rho_{\rm vap}(z)\ dz$, and $L = \int \rho_{\rm liq}(z)\ dz$, where $\rho_{\rm vap}$ is the water vapor mass density, V is the integrated water vapor, $\rho_{\rm liq}$ is the mass of liquid water per unit volume of cloud, and L is the integrated cloud liquid water. It follows that $\bar{\kappa}_{\rm vap} = \tau_{\rm vap}/V$ and $\bar{\kappa}_{\rm liq} = \tau_{\rm liq}/L$ with units of $\rm m^2/g$. It is common practice to normalize V and L by the nominal density of liquid water, 10^3 $\rm kg/m^3$, such that these quantities have units of length and represent the height of an equivalent column of liquid water. As such, V is known as the precipitable water vapor (PWV), or simply the precipitable water, and L is known as the liquid water path (LWP). For PWV and LWP in millimeters, $\bar{\kappa}$ would have units of inverse millimeters. The frequency-dependent opacity may now be written as

$$\tau = \tau_{\rm dry} + \bar{\kappa}_{\rm vap} V + \bar{\kappa}_{\rm liq} L. \tag{2}$$

The dry contribution is then subtracted to yield

$$\tau^* = \tau - \tau_{\rm dry} = \bar{\kappa}_{\rm vap} V + \bar{\kappa}_{\rm liq} L, \tag{3}$$

and the two equations (one for each measurement frequency) corresponding to (3) are solved for V and L as

$$V = v_1 \tau_1^* + v_2 \tau_2^*, \tag{4a}$$
$$L = l_1 \tau_1^* + l_2 \tau_2^*, \tag{4b}$$

where the retrieval coefficients are given by

$$v_1 = \left(\bar{\kappa}_{\rm vap,1} - \bar{\kappa}_{\rm vap,2}\ \frac{\bar{\kappa}_{\rm liq,1}}{\bar{\kappa}_{\rm liq,2}}\right)^{-1}, \tag{5a}$$

$$-v_2 = \left(\bar{\kappa}_{\rm vap,1}\ \frac{\bar{\kappa}_{\rm liq,2}}{\bar{\kappa}_{\rm liq,1}} - \bar{\kappa}_{\rm vap,2}\right)^{-1}, \tag{5b}$$

$$-l_1 = \left(\bar{\kappa}_{\rm liq,2}\ \frac{\bar{\kappa}_{\rm vap,1}}{\bar{\kappa}_{\rm vap,2}} - \bar{\kappa}_{\rm liq,1}\right)^{-1}, \tag{5c}$$

$$l_2 = \left(\bar{\kappa}_{\rm liq,2} - \bar{\kappa}_{\rm liq,1}\ \frac{\bar{\kappa}_{\rm vap,2}}{\bar{\kappa}_{\rm vap,1}}\right)^{-1}. \tag{5d}$$

Here the subscripts "vap" and "liq" refer to vapor and liquid absorption, respectively, and the subscripts "1" and "2" refer to the vapor- and liquid-sensitive frequencies, 23.8 and 31.4 GHz, respectively.

At each frequency the sky brightness temperature $T_{\rm sky}$ measured by a microwave radiometer can be expressed in terms of extraterrestrial and atmospheric contributions:

$$T_{\rm sky} = T_c e^{-\tau} + T_{mr}\left(1 - e^{-\tau}\right). \tag{6}$$

Here $T_{\rm c}$ is the cosmic background radiating temperature (2.73 K), and T_{mr} is the mean atmospheric radiating temperature defined as

$$T_{mr} = \frac{\int_0^\infty T(z)\ w(z)\ dz}{\int_0^\infty w(z)\ dz}, \tag{7}$$

where

$$w(z) = \alpha(z)\ e^{-\int_0^z \alpha(z')\ dz'} \tag{8}$$

and $\alpha = \kappa_{\rm dry}\rho_{\rm dry} + \kappa_{\rm vap}\rho_{\rm vap} + \kappa_{\rm liq}\rho_{\rm liq}$ is the volume absorption coefficient. By rearranging (6) the opacity can be calculated from the measured sky brightness temperature $T_{\rm sky}$:

$$\tau = \ln\left(\frac{T_{mr} - T_{\rm c}}{T_{mr} - T_{\rm sky}}\right). \tag{9}$$

Because V and L depend linearly on opacity (4), whereas the relationship between the opacity and brightness temperature is (weakly) nonlinear (6), it is preferable to develop the retrieval in terms of opacity and to transform the measured brightness temperatures to opaci-

ties via (9) rather than to relate V and L directly to the measured brightness temperatures. Note that the parameter T_{mr} must be estimated in the retrieval procedure.

2.2. Site-Specific Statistical Retrieval

In a site-specific statistical retrieval the relationship between the opacities and the retrieved PWV and LWP are determined by linear regression over a large data set, usually consisting of prior radiosonde soundings launched at or near the desired location, as

$$\hat{V} = v_0 + v_1\tau_1 + v_2\tau_2, \quad (10a)$$

$$\hat{L} = l_0 + l_1\tau_1 + l_2\tau_2. \quad (10b)$$

Mean values of T_{mr} (one for each frequency) are used in (9) to calculate τ_1 and τ_2 from the brightness temperatures. The contribution from τ_{dry} is included in the v_0 and l_0 coefficients. Because the retrieval coefficients v_i and l_i are constants, τ_{dry} and the path-averaged mass absorption coefficients $\bar{\kappa}$ are treated as constants in a site-specific statistical retrieval, even though the latter coefficients depend on temperature, barometric pressure, and vapor pressure. To achieve a reasonably accurate result with this method, common practice is to compute retrieval coefficients and mean radiating temperatures for monthly subsets of the a priori site-specific data set to account for gross variations in the underlying parameters over the course of an annual cycle.

The chief advantages of this method are its simplicity and reasonable accuracy, especially for PWV. The chief drawbacks of this method are that it requires a large a priori data set for the specific location where it will be applied, it is only valid for that specific location, and it cannot account for actual variations in the underlying parameters. This is especially problematic for LWP because the values of $\bar{\kappa}_{\text{liq}}$ depend on the temperature of the cloud and thus on its height and vertical extent.

2.3. Development of a New Site-Independent Statistical Retrieval

In the new retrieval the mean radiating temperature T_{mr}, the oxygen contribution τ_{dry}, and the retrieval coefficients v_1, v_2, l_1, and l_2 are estimated from measurements of surface temperature, barometric pressure, vapor pressure or relative humidity, and (for l_1 and l_2) T_{cloud} each time the retrieval is to be applied. Extensive radiosonde data from ARM, the Tropical Ocean Global Atmosphere (TOGA) Coupled Ocean Atmosphere Research Experiment (COARE), the National Weather Service (NWS), and the Surface Heat Budget of the Arctic (SHEBA) program were used to develop estimators for these parameters. As Table 1 shows, the sites from which the soundings were drawn experience a wide range of atmospheric conditions from polar (Barrow and Arctic ice pack) to tropical (Manus Island, Papua New Guinea) to midcontinental (Oklahoma and Kansas) and from near sea level (Barrow, Arctic ice pack, and Manus Island) to approximately 1600 m above sea level (Albuquerque). In this way, the full range of the parameter space for the retrieval is covered.

Each sounding was integrated to determine V. Because radiosondes do not measure liquid water, clouds were inserted into each profile for up to three layers where the relative humidity over liquid water exceeded 95% [*Decker et al.*, 1978]. Soundings for which the relative humidity did not exceed 95% at any point were classified as clear; the remaining soundings were classified as cloudy (Table 1). For each "cloudy" radiosonde, three liquid water profiles were produced, corresponding to high, medium, and low liquid water concentrations, in order to create a realistic range of liquid water distributions, integrated amounts L, and mean cloud liquid water temperatures T_{cloud}. Thus the number of cloudy profiles is 3 times the number of cloudy soundings.

Each profile was then input to a microwave radiative transfer model [*Schroeder and Westwater*, 1991]. This model is based on the MPM87 microwave absorption model [*Liebe and Layton*, 1987]. The model assumes that the cloud droplets are small relative to the measurement wavelengths (i.e., they obey the Rayleigh limit). The scattering effects of large droplets (greater than 100 μm) associated with precipitation are not included in the model. Consequently, our retrieval does not apply to precipitating conditions. In addition, any errors or deficiencies in the absorption model will affect the retrieval; however, because the retrieval coefficients (5) have opposite signs at the two measurement fre-

Table 1. Distribution of Soundings

Site	Source	N_{clear}	N_{cloudy}	P_{sfc}, hPa	T_{sfc}, K	V, mm
Arctic Ice Pack	SHEBA	353	361	1015±16[a]	256±16[a]	9± 7[a]
Barrow, Alaska	NWS	751	969	1017±17	260±19	10± 9
Manus Is., Papua New Guinea	TOGA	632	57	1009± 3	300± 3	50±10
Morris, Oklahoma	ARM	1594	648	990±10	293±15	27±21
Lamont, Oklahoma	ARM	3910	1641	978±11	289±18	25±20
Purcell, Oklahoma	ARM	1150	474	974±10	292±18	26±19
Hillsboro, Kansas	ARM	1531	558	964±11	291±16	24±17
Vici, Oklahoma	ARM	1020	342	943±10	293±15	23±16
Albuquerque, New Mexico	NWS	2534	553	838± 7	289±16	17±12

[a]Median ± (95th percentile to 5th percentile)/2.

Table 2. Regression Equations and Parameters

$\hat{T}_{mr} = a + b\ T_{\rm sfc} + c\ RH_{\rm sfc}$ (11)

$\hat{\tau}_{\rm dry} = a + b\ (P_{\rm sfc} - e_{\rm sfc})^2/T_{\rm sfc}$ (13)

$\hat{v} = a + b\ P_{\rm sfc} + c_1\ T_{\rm sfc} + c_2\ T_{\rm sfc}^2 + d_1\ e_{\rm sfc} + d_2\ e_{\rm sfc}^2$ (14)

$\hat{l} = a + b\ P_{\rm sfc} + \exp(c_1 + c_2\ T_{\rm cloud})$ (17)

$\hat{l} = a + b\ P_{\rm sfc} + c\ P_{\rm sfc}\ e_{\rm sfc} + d\ e_{\rm sfc}^2$ (19)

For equation (11)	a, K	b, K/K	c, K			R^2	RMSE, K
$\hat{T}_{\rm mr,23.8}$	39.3689	0.793578	0.125758			0.909	3.41
$\hat{T}_{\rm mr,31.4}$	34.1744	0.792481	0.167245			0.893	3.70
For equation (13)	a, –	b, K/bar^2				R^2	RMSE, –
$\hat{\tau}_{\rm dry,23.8}$	0.000842	3.96326				0.975	0.0003
$\hat{\tau}_{\rm dry,31.4}$	0.001347	6.68708				0.975	0.0005
For equation (14)	a, mm	b, $\frac{\rm mm}{\rm hPa}$	c_1, $\frac{\rm mm}{\rm K}$	c_2, $\frac{\rm mm}{\rm K^2}$	d_1, $\frac{\rm mm}{\rm hPa}$	d_2, $\frac{\rm mm}{\rm hPa^2}$	RMSE, mm
$\hat{v}_1$	370.676	0.101635	-1.61249	0.002653	0.565695	-0.008588	4.16
$-\hat{v}_2$	426.011	0.050704	-2.32457	0.003963	0.146403	-0.001546	2.58
For equation (17)	a, mm	b, $\frac{\rm mm}{\rm hPa}$	c_1, –	c_2, K^{-1}		R^2	RMSE, mm
$-\hat{l}_1$	-2.1728	0.002618	-7.24277	0.028984		0.965	0.123
$\hat{l}_2$	-1.5338	0.001577	-3.85181	0.021283		0.997	0.083
For equation (19)	a, mm	b, $\frac{\rm mm}{\rm hPa}$	c, $\frac{\rm mm}{\rm hPa^2}$	d, $\frac{\rm mm}{\rm hPa^2}$		R^2	RMSE, mm
$-\hat{l}_1$	-2.75671	0.004317	0.000129	-0.002482		0.558	0.438
$\hat{l}_2$	-1.33514	0.006140	0.000358	-0.007339		0.551	1.109

quencies, any changes in the model which result in a general increase or decrease in the brightness temperatures will tend to offset each other to an extent in the retrieval. For example, a 0.5 K increase in $T_{\rm sky}$ at 31.4 GHz will result in an increase in the retrieved LWP of 0.01-0.02 mm, whereas a 0.5 K increase at both 31.4 and 23.8 GHz will cause the LWP to increase by only half as much, 0.005-0.01 mm.

We used the model to calculate the three components of opacity (i.e., $\tau_{\rm dry}$, $\tau_{\rm vap}$, and $\tau_{\rm liq}$), as well as the mean radiating temperature T_{mr} and sky brightness temperature $T_{\rm sky}$ at the two measurement frequencies of 23.8 and 31.4 GHz. For each profile, the calculated values for V and $\tau_{\rm vap}$ are used to compute $\bar{\kappa}_{\rm vap}$, and L and $\tau_{\rm liq}$ yield $\bar{\kappa}_{\rm liq}$. Then $\bar{\kappa}_{\rm vap}$ and $\bar{\kappa}_{\rm liq}$ are used to calculate v_1, v_2, l_1, and l_2 via (5). Once these calculations are completed for all of the profiles, the values of v_1, v_2, l_1, and l_2, as well as T_{mr} and $\tau_{\rm dry}$, are regressed against surface temperature, barometric pressure, vapor pressure or relative humidity, and (for l_1 and l_2) $T_{\rm cloud}$ to develop the necessary estimators. The calculated values of $T_{\rm sky}$ are used to simulate a radiometer and test the retrieval algorithms.

2.3.1. Mean radiating temperature (T_{mr}) estimation. The mean radiating temperature at each frequency correlates well with the temperature and relative humidity at the surface because the weighting function (8) is a maximum at the surface and decreases rapidly with height for clear-sky conditions. Clouds can significantly affect the weighting function, however. The mean radiating temperature was fitted by linear regression to the estimator

$$\hat{T}_{mr} = a + b\ T_{\rm sfc} + c\ RH_{\rm sfc}. \qquad (11)$$

The regression parameters, derived by using all clear and cloudy profiles, are summarized in Table 2, in which $RH_{\rm sfc}$ is the fractional relative humidity, ranging from 0 to 1. Although T_{mr} depends primarily on $T_{\rm sfc}$, the correlation with $RH_{\rm sfc}$ substantially reduces the root-mean-square error (RMSE), especially for cloudy conditions. With this relationship, T_{mr} can be estimated with approximately 1% RMSE for a wide range of locations and sky conditions.

Because the estimator (11) relies on surface conditions, it is subject to error when the surface conditions become decoupled from the atmospheric column, such as during near-surface temperature inversions. For instances where the surface air temperature is less than the air temperature at 1 km above the ground, a bias of 2-3 K, or 1%, arises with this estimator. This bias results in an average bias error of 0.2-0.3 mm in the retrieved PWV and about -0.01 mm in LWP.

2.3.2. Oxygen opacity ($\tau_{\rm dry}$) estimation. With (1) and the hydrostatic equation, the "dry" contribution to the opacity due to oxygen can be expressed as

$$\tau_{\rm dry} = (w_{\rm O_2}/g)\ (P_{\rm sfc} - e_{\rm sfc})\ \bar{\kappa}_{\rm O_2}. \qquad (12)$$

Here w_{O_2} is the (constant) mixing ratio of oxygen, P_{sfc} is the surface barometric pressure, e_{sfc} is the surface partial pressure due to water vapor, and g is the acceleration due to gravity. The path-averaged mass absorption coefficient $\bar{\kappa}_{O_2}$ is proportional to $(P_{sfc} - e_{sfc})/T_{sfc}$, which reflects the contributions of the far wings of the oxygen lines centered around 60 GHz and nonresonant absorption due to oxygen [*Rosenkranz*, 1993]. T_{sfc} is the surface absolute temperature. Using surface values of pressure, temperature, and relative humidity from the soundings, τ_{dry} was fitted to the estimator

$$\hat{\tau}_{dry} = a + b\,(P_{sfc} - e_{sfc})^2/T_{sfc}, \tag{13}$$

as summarized in Table 2. The RMSE represents about 2% of the mean for each frequency. At all locations in the current study, the scatter about the fit increases with decreasing temperature because of meteorological conditions, such as temperature inversions, for which the surface data are less representative of the vertical column. For instances where the surface air temperature is less than the air temperature at 1 km above the ground, a bias of about 1% occurs. The effect of this bias on the retrieved LWP and PWV is generally negligible, in part because the retrieval coefficients have opposite signs, and in part because the oxygen contribution to the brightness temperatures is often (but not always) small relative to the vapor and liquid water contributions.

2.3.3. Water vapor retrieval coefficient (v_1, v_2) estimation. The vapor-sensing frequency for the microwave radiometer is displaced from the center of the water vapor resonance at 22.235 GHz to 23.8 GHz, where the Van Vleck-Weisskopf line shape is minimally sensitive to changes in pressure. The advantage of this displacement is that the mass absorption coefficient, which depends on the line shape, varies only slightly with height, so τ_{vap} at 23.8 GHz is not sensitive to the vertical distribution of water vapor but varies only in proportion to the total water vapor amount. For this reason and because variations in local barometric pressure are a small fraction of the mean pressure, variations in the path-averaged mass absorption coefficient $\bar{\kappa}_{vap,1}$ are negligibly correlated with barometric pressure for any given location. In contrast, weak correlations are apparent with surface temperature and vapor pressure because of their influence on the line intensity, line half width, and water vapor continuum [*Rosenkranz*, 1993].

At the liquid-sensing frequency of 31.4 GHz the contribution to the path-averaged mass absorption coefficient from the wing of the 22.235-GHz water vapor resonance is less than that at 23.8 GHz by about a factor of 6 and often less than the contribution from the water vapor continuum. With the water vapor continuum included, the contribution of water vapor at 31.4 GHz is still less than that at 23.8 GHz by about a factor of 3. Even though the water vapor continuum depends on barometric pressure, vapor pressure, and temperature, variations in $\bar{\kappa}_{vap,2}$ are negligibly correlated with barometric pressure variations for any given site, because variations in surface pressure about the mean are small, whereas noticeable correlations exist with surface temperature and vapor pressure. However, large changes in mean barometric pressure from site to site, associated with different site elevations, result in noticeably different values of $\bar{\kappa}_{vap,1}$ and $\bar{\kappa}_{vap,2}$ for each location. For v_1 and v_2 to be site-independent, this pressure dependence needs to be taken into account, in addition to the correlations with surface temperature and vapor pressure.

With the above effects in mind, the estimator that we developed for v is

$$\hat{v} = a + b\,P_{sfc} + c_1\,T_{sfc} + c_2\,T_{sfc}^2 + d_1\,e_{sfc} + d_2\,e_{sfc}^2. \tag{14}$$

The RMSE of the regression (14) represents 2% or less of the mean values of v_1 and v_2 for any site (Table 2). Because the integrated liquid amount appears in the denominator of (1), the path-averaged mass absorption coefficients and the corresponding values of the retrieval coefficients were computed by using only cloudy soundings.

2.3.4. Liquid water retrieval coefficient (l_1, l_2) estimation. Retrieval of the integrated liquid water amount L is complicated by the fact that $\bar{\kappa}_{liq}$ varies exponentially with the liquid-water-weighted mean temperature of the cloud,

$$T_{cloud} = \int_{z_{base}}^{z_{top}} T(z)\,w(z)\,dz, \tag{15}$$

where

$$w(z) = \rho_{liq}(z)/L. \tag{16}$$

The relationship between $\bar{\kappa}_{liq}$ and T_{cloud} is the same for all locations, as well as for single- and multiple-layer clouds. Because $\bar{\kappa}_{liq}$ depends exponentially on T_{cloud}, so do the liquid water retrieval coefficients l_1 and l_2 (Figure 1). The water vapor retrieval coefficients v_1 and v_2 do not exhibit a similar dependence on T_{cloud} because the ratio $\bar{\kappa}_{liq,1}/\bar{\kappa}_{liq,2}$ is independent of T_{cloud}. As Figure 1 also demonstrates, the dependence of l_1 and l_2 on barometric pressure is nonnegligible due to the pressure dependence of the ratio $\bar{\kappa}_{vap,1}/\bar{\kappa}_{vap,2}$. Accordingly, l_1 and l_2 have been fitted to the estimator

$$\hat{l} = a + b\,P_{sfc} + \exp(c_1 + c_2\,T_{cloud}), \tag{17}$$

as summarized in Table 2.

2.3.5. Liquid-water-weighted mean cloud temperature (T_{cloud}) estimation. The mean cloud temperature T_{cloud} is difficult to determine because it depends on the vertical distribution of temperature and liquid water in the cloud. Initially, we tried using a simple infrared detector at a wavelength of 10 μm to estimate cloud temperature. We encountered three problems with this approach. First, the emissivity of thin clouds can be less than 1.0 at 10 μm, which results in

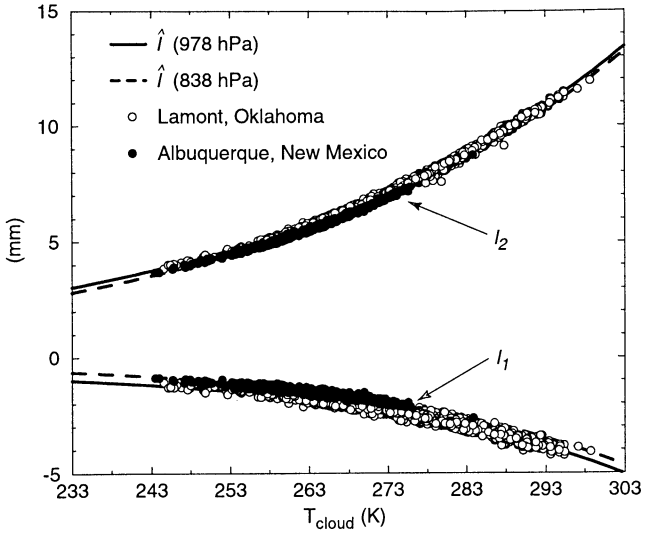

Figure 1. Values of the liquid water path retrieval coefficients l_1 and l_2 for Lamont, Oklahoma ($\langle P_{sfc} \rangle$ = 978 hPa), and Albuquerque, New Mexico ($\langle P_{sfc} \rangle$ = 838 hPa), as a function of T_{cloud}, the liquid-water-weighted mean cloud temperature. The estimators $\hat{l}_1$ and $\hat{l}_2$ for these values of surface pressure are also shown.

an underestimate of T_{cloud}. Second, because the liquid water distribution generally increases with height in the cloud, for thick clouds, T_{cloud} can be substantially less than the cloud base temperature reported by the infrared detector. Finally, the contribution from water vapor to the infrared measurement at 10 μm can be significant, which causes an overestimate of T_{cloud}.

The approach taken here is to use a collocated cloud radar to estimate $w(z)$ and radiosondes or remote sensing systems to estimate $T(z)$ and to combine these estimates according to (15) to estimate T_{cloud}. The radar reflectivity Z is proportional to the sixth moment of the cloud droplet size distribution, whereas ρ_{liq} is proportional to the third moment. *Frisch et al.* [1998] showed that the square of the third moment is linearly proportional to the sixth moment for a wide range of in situ measurements of cloud droplet size distributions (provided that the droplet number density and the spread of the distribution are constant with height) and for the lognormal and gamma distributions often used to model droplet size distributions. Thus we set

$$w(z) = Z(z)^{1/2}. \tag{18}$$

2.3.6. Retrieval of liquid water path without an estimate of T_{cloud}. It is possible to estimate l_1 and l_2 without an estimate of T_{cloud} by using a relationship of the form

$$\hat{l} = a + b\ P_{sfc} + c\ P_{sfc}\ e_{sfc} + d\ e_{sfc}^2, \tag{19}$$

as summarized in Table 2. The P term reflects the influence of the pressure-broadened wing of the 22-GHz water vapor line, the mixed $P-e$ term reflects the influence of the foreign-broadened water vapor continuum, and the term e_{sfc}^2 reflects the influence of the self-broadened continuum. The R^2 statistic shows that this regression explains only about half of the variance in l_1 and l_2, whereas the regression that uses T_{cloud} explains nearly all of the variance. The only advantage of this retrieval is that it permits reasonably accurate estimates of L to be obtained without a cloud radar and without the a priori data set and the effort needed to develop a site-specific statistical retrieval. Consequently, it can be used as a default for periods when radar data are unavailable.

2.4. Theoretical Basis of the Iterative Physical Retrieval

To assess the performance of the current site-specific and new site-independent statistical retrievals for LWP, we developed an iterative physical retrieval method for estimation of both LWP and PWV from the dual-frequency brightness temperature measurements obtained with the ARM microwave radiometers. In the iterative retrieval we used the same microwave radiative transfer model [*Schroeder and Westwater,* 1991] which we used to develop the site-specific and site-independent statistical retrievals to explicitly compute the surface downwelling brightness temperatures, given the best observational data on the state of the atmosphere at the time of the measurements. Radiosondes provided information about the vertical distribution of temperature and moisture, while millimeter-wave cloud radar reflectivity measurements provided a means (18) for estimating the vertical distribution of cloud liquid water. Others [*Han and Westwater,* 1995] have used lidar measurements of cloud base height in an iterative physical retrieval to improve estimates of V and L.

To initiate the iterative retrieval, the relative humidity profiles from the radiosondes and the radar-derived liquid water content profiles were first scaled to agree with the PWV and LWP values derived from the microwave radiometer brightness temperature measurements by using the currently implemented site-specific retrievals. These scaled profiles were subsequently input to the model to compute the brightness temperatures at 23.8 and 31.4 GHz. Differences between the two model-calculated brightness temperatures and those observed were computed and, if the magnitude of either difference was more than 0.3 K (the RMS uncertainty of the microwave radiometer brightness temperature measurements), an iterative scheme was entered whereby PWV and LWP were adjusted (by multiplying the relative humidity and liquid water content values in the input vertical profiles by some value close to 1) until the model-measured differences were made sufficiently small. Because the primary goal of the iterative retrieval was to obtain accurate LWP, we forced the solution to greater accuracy in the 31.4-GHz channel while still requiring agreement in both channels to within the RMS un-

certainty of the radiometer measurements. Typically, 20-50 iterations were required for convergence, and the scheme was stopped if no solution was found after 100 iterations. Although this method might yield the most accurate results, clearly it has only limited practicality, an example being our use of it to evaluate the new site-independent retrieval.

The RMS uncertainties in the retrieved PWV and LWP were next obtained by perturbing the brightness temperatures measured with the radiometer by 0.3 K and solving again for the retrieved PWV and LWP. Because the iterative retrieval scheme is computationally expensive, we did not examine all combinations of the 0.3 K perturbation. Rather, we drove the perturbed solution as far from the original one as possible by adding 0.3 K to one channel and subtracting it from the other. This process was repeated (but with a change in sign of the perturbation) for each channel brightness temperature, and the largest differences between the two resulting sets of PWV and LWP from the original retrieved values were interpreted as the maximum possible error. Because the error most likely lies somewhere between zero and the maximum that we calculated, we took one half of the maximum value as an estimate of the RMS uncertainty in the original retrieval values.

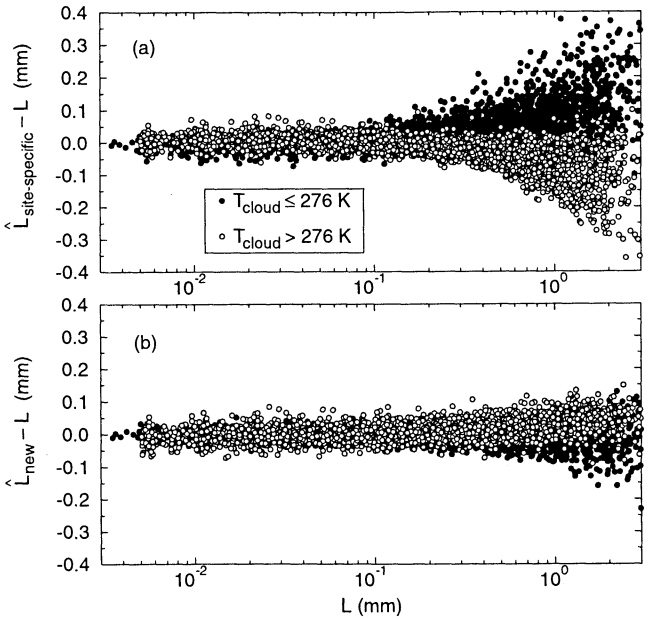

Figure 2. Errors ($\Delta L = \hat{L} - L$) in simulated measurements for (a) the current site-specific statistical retrieval and (b) the new site-independent retrieval as a function of the combined values of L from Lamont, Oklahoma; Purcell, Oklahoma; and Hillsboro, Kansas, all of which are at nearly the same elevation. Cases when $T_{cloud} > \langle T_{cloud} \rangle$ are indicated by open circles, while cases when $T_{cloud} \leq \langle T_{cloud} \rangle$ are indicated by solid circles.

3. Results

We evaluated the performance of the new site-independent retrieval by using both simulated and real measurements. The simulated measurements were constructed from the set of radiosondes also used to develop the new retrieval. Although this procedure does not provide an independent evaluation of the new retrieval, it nevertheless gives insight into the performance of the new retrieval and permits comparison of its performance with that of site-specific retrievals. As described earilier, profiles of cloud liquid water were constructed by inserting three different distributions of cloud liquid water into each sounding where the relative humidity exceeded 95%. Using these profiles of temperature, relative humidity, and cloud liquid water, we computed the "true" values of LWP and PWV for comparison with the retrieved values; values of T_{cloud} were also computed. The profiles were input to the radiative transfer model to calculate the microwave brightness temperatures at 23.8 and 31.4 GHz. To simulate a radiometer, Gaussian-distributed noise (mean zero, $\sigma_{T_{sky}} = 0.3$ K)

Table 3. Comparison of Liquid Water Path From Site-Independent and Site-Specific Retrievals Using Simulated Brightness Temperature Measurements

	$L \leq 0.25$ mm				$L > 0.25$ mm			
	Site-Independent Retrieval		Site-Specific Retrieval		Site-Independent Retrieval		Site-Specific Retrieval	
Site	$\langle \Delta L \rangle$	$\sigma_{\Delta L}$	$\langle \Delta L \rangle$	$\sigma_{\Delta L}$	$\langle \Delta L \rangle$	$\sigma_{\Delta L}$	$\langle \Delta L \rangle$	$\sigma_{\Delta L}$
SHEBA	0.001	0.008	0.002	0.012	0.011	0.018	0.026	0.057
Barrow, Alaska	0.002	0.009	0.001	0.011	0.019	0.025	0.002	0.041
Manus Is., Papua New Guinea	0.003	0.020	0.004	0.019	-0.003	0.025	-0.006	0.073
Morris, Oklahoma	0.003	0.022	0.016	0.021	0.012	0.035	0.003	0.088
Lamont, Oklahoma	-0.002	0.018	0.005	0.020	0.008	0.032	0.005	0.086
Purcell, Oklahoma	0.003	0.021	0.005	0.020	0.010	0.032	-0.004	0.092
Hillsboro, Kansas	-0.003	0.016	-0.002	0.021	0.006	0.029	0.012	0.088
Vici, Oklahoma	-0.005	0.018	-0.014	0.021	0.007	0.030	-0.010	0.088
Albuquerque, New Mexico	-0.001	0.009	-0.001	0.014	-0.011	0.023	-0.009	0.055

$\Delta L = \hat{L} - L$. $\langle \Delta L \rangle$ and $\sigma_{\Delta L}$, respectively, indicate the ensemble average and standard deviation. All values are in units of millimeters.

was added to the model-calculated brightness temperatures, which served as input to both the site-specific and new site-independent retrievals. Gaussian-distributed noise (mean zero, $\sigma_{T_{\text{cloud}}} = 0.5$ K) was also added to the values of T_{cloud} to simulate actual measurements.

On the four case study days, the true values of PWV and LWP are unknown. We treat the iterative physical retrieval results as representing the truth and test the skill of the site-specific and site-independent retrievals relative to it.

The evaluation of the new LWP retrieval is presented below. The evaluation of the PWV retrieval is presented in Appendix A.

3.1. Comparison of Site-Independent and Site-Specific Retrievals

To assess the skill of the new retrieval for liquid water path, opacities were calculated from the simulated brightness temperature measurements according to (9) by using the estimators for T_{mr}, then the values of τ_{dry} were estimated using the surface parameters and subtracted. The simulated measurements of T_{cloud} and the surface pressure were used to estimate l_1 and l_2 using (17).

3.1.1. Results for cloudy-sky conditions. The differences $\Delta L = \hat{L} - L$ between the retrieval estimates, $\hat{L}$, and the true values, L, from the simulation data set are plotted as a function of L in Figure 2 for Lamont, Oklahoma, Purcell, Oklahoma, and Hillsboro, Kansas. These three sites are at nearly the same elevation as Oklahoma City, Oklahoma, for which the current site-specific retrieval was developed. (The current retrieval exhibits biases at Morris and Vici because the site elevations, and thus the barometric pressures, are significantly different from Oklahoma City for which the retrieval was developed.) The corresponding statistics (Table 3) reveal that both retrievals yield unbiased estimates of L. For values of L greater than 0.25 mm (approximately the median value of L in the simulation data set for these sites) the standard deviation of ΔL, $\sigma_{\Delta L}$, is reduced on average by about a factor of 3 when the actual value of T_{cloud} is used to determine l_1 and l_2 rather than the ensemble average value, $\langle T_{\text{cloud}} \rangle$, of 276 K for these three sites implied by the constant coefficients for the site-specific retrieval. Because the actual site-specific retrieval coefficients are developed for monthly subsets of the a priori data set, $\langle T_{\text{cloud}} \rangle$ actually varies between 268-281 K for these sites. However, monthly plots corresponding to Figure 2a would show a very similar result. For $L \leq 0.25$ mm, using the actual value of T_{cloud} appears to yield little improvement. Large errors in $\bar{\kappa}_{\text{liq}}$ do not result in large errors in $\hat{L}$ when L is small.

Figure 2a also reveals that for $L > 0.25$ mm the current site-specific retrieval overestimates L when $T_{\text{cloud}} \leq \langle T_{\text{cloud}} \rangle$ and underestimates L when $T_{\text{cloud}} > \langle T_{\text{cloud}} \rangle$.

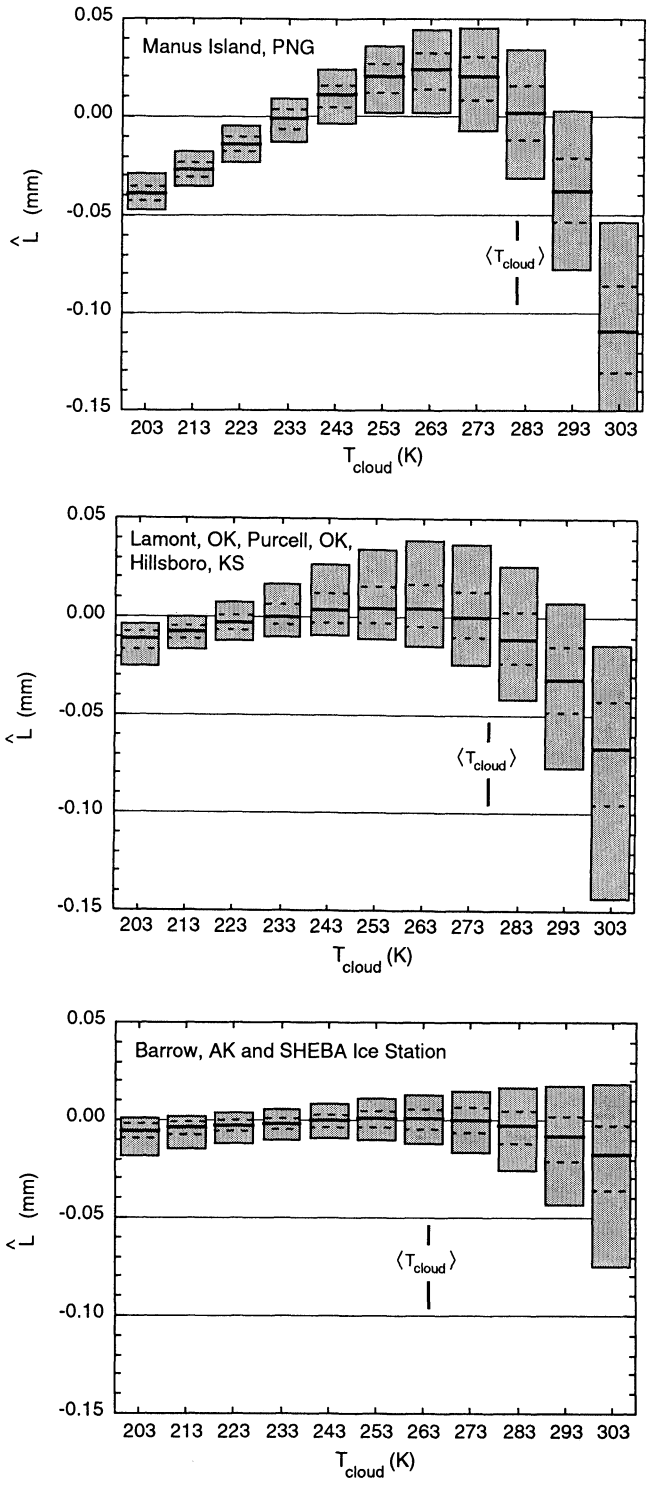

Figure 3. Distributions of $\hat{L}$ from simulations calculated by using fixed values of T_{cloud} for cases where $L = 0$. (top) Tropical site (Manus Island, Papua New Guinea); (middle) midlatitude sites (Lamont, Oklahoma; Purcell, Oklahoma; and Hillsboro, Kansas); (bottom) polar sites (Barrow, Alaska, and SHEBA ice station). Each box spans the range from the 5th to the 95th percentiles. The thick solid lines indicate the medians, while the dashed lines indicate the 25th and 75th percentiles. The value of $\langle T_{\text{cloud}} \rangle$ for each location is indicated.

If $T_{\text{cloud}} \leq \langle T_{\text{cloud}} \rangle$, then the average value of $\bar{\kappa}_{\text{liq}}$ implied by the site-specific retrieval will be smaller than the actual value of $\bar{\kappa}_{\text{liq}}$, and $\hat{L}$ from the site-specific retrieval will be larger than L.

By incorporating T_{cloud} the new site-independent retrieval largely overcomes these problems (Figure 2b), although increasing error is evident for $L > 1$ mm. When $T_{\text{cloud}} > 276$ K, positive differences $(\hat{L} - L)$ arise because of underestimation of the mean radiating temperature T_{mr}. Conversely, for $T_{\text{cloud}} \leq 276$ K, negative differences arise because of overestimation of T_{mr}. For large values of L, T_{mr} is not so well correlated with the surface temperature as it is when $L < 1$ mm, because the cloud significantly affects the T_{mr} weighting function (8); errors in $\hat{T}_{mr}$ increase with increasing cloud base height. Computations have shown that if the surface relative humidity is not included in (11) and only the surface temperature is used, the errors in $\hat{L}$ are approximately twice as great. Of greater concern perhaps is the fact that values of $L > 1$ mm are frequently accompanied by precipitation. Simulation studies [*Sheppard*, 1996] have demonstrated that LWP retrievals that rely on the Rayleigh assumption as ours does can overestimate the true LWP when large droplets (i.e., radius greater than 100 μm) are present, such as during precipitation. The degree of overestimation depends mainly on the rain layer depth and rainfall rate. Nevertheless, the new retrieval still offers substantially improved accuracy for large liquid water paths under nonprecipitating conditions.

A more accurate microwave radiometer will do little to improve the accuracy of the retrieved LWP. The simulated instrument error (i.e., the Gaussian noise added to the brightness temperatures) contributes only about 20% to the total error in $\hat{L}$ for $L \leq 0.25$ mm. For $L > 0.25$ mm, the contribution of the simulated instrument error to the values of the standard deviation in Table 3 is less than 5%. The bulk of the error in $\hat{L}$ arises from errors in the underlying estimators for T_{mr}, τ_{dry}, l_1, and l_2.

3.1.2. Results for clear-sky conditions. Perhaps the most striking difference in $\hat{L}$ between the two retrievals is for clear-sky conditions. To understand the behavior of the site-specific retrieval for these conditions, it is helpful to view the site-specific retrieval as equivalent to the site-independent retrieval but with the underlying parameters fixed at their average values for the a priori data set. This means that l_1 and l_2 are fixed according to the values of $\langle T_{\text{cloud}} \rangle$ and $\langle P_{\text{sfc}} \rangle$. Because $\hat{L} = l_1 \tau_1^* + l_2 \tau_2^*$, for $\hat{L}$ to be equal to zero, $-l_1 \tau_1^*$ must equal $l_2 \tau_2^*$ exactly. Deviations of the actual values of T_{mr} or τ_{dry} from their average values lead to errors in τ_1^* and τ_2^*, resulting in a nonzero value for $\hat{L}$. Moreover, l_1 and l_2 increase in magnitude as $\langle T_{\text{cloud}} \rangle$ and $\langle P_{\text{sfc}} \rangle$ increase (Figure 1). As l_1 and l_2 increase in magnitude, the sensitivity of the LWP retrieval to errors also increases. In addition, because τ^* increases in proportion to V, nonzero values of $\hat{L}$ will also increase with V. Thus the range of nonzero values of $\hat{L}$ from a site-specific statistical retrieval during clear-sky conditions will be considerably larger at tropical sites, for example, where $\langle T_{\text{cloud}} \rangle$ and V are relatively large, than for polar sites where $\langle T_{\text{cloud}} \rangle$ and V are much smaller.

Distributions of $\hat{L}$ for the simulated measurements for clear-sky conditions ($L = 0$) are presented in Figure 3 as a function of T_{cloud} for tropical, midlatitude, and polar sites. The value of $\langle T_{\text{cloud}} \rangle$ for each location is indicated by a vertical bar. For the polar sites (bottom), $\langle T_{\text{cloud}} \rangle = 264$ K, and the difference between the 95th and the 5th percentile in the $\hat{L}$ distribution is 0.013 mm. For the midlatitude sites (middle), these values increase to 276 K and 0.035 mm, respectively. For the tropical

Table 4. Comparison of Liquid Water Path From Site-Independent Retrieval Without T_{cloud} and Site-Specific Retrievals Using Simulated Brightness Temperature Measurements

	$L \leq 0.25$ mm				$L > 0.25$ mm			
	Site-Independent Retrieval		Site-Specific Retrieval		Site-Independent Retrieval		Site-Specific Retrieval	
Site	$\langle \Delta L \rangle$	$\sigma_{\Delta L}$	$\langle \Delta L \rangle$	$\sigma_{\Delta L}$	$\langle \Delta L \rangle$	$\sigma_{\Delta L}$	$\langle \Delta L \rangle$	$\sigma_{\Delta L}$
SHEBA	0.004	0.013	0.002	0.012	0.019	0.050	0.026	0.057
Barrow, Alaska	0.005	0.013	0.001	0.011	0.022	0.044	0.002	0.041
Manus Is., Papua New Guinea	-0.015	0.021	0.004	0.019	0.031	0.089	-0.006	0.073
Morris, Oklahoma	0.004	0.021	0.016	0.021	0.039	0.103	0.003	0.088
Lamont, Oklahoma	-0.002	0.020	0.005	0.020	0.026	0.097	0.005	0.086
Purcell, Oklahoma	0.000	0.021	0.005	0.020	0.024	0.102	-0.004	0.092
Hillsboro, Kansas	0.003	0.021	-0.002	0.021	0.013	0.088	0.012	0.088
Vici, Oklahoma	-0.005	0.019	-0.014	0.021	-0.010	0.087	-0.010	0.088
Albuquerque, New Mexico	-0.002	0.013	-0.001	0.014	-0.015	0.066	-0.009	0.055

$\Delta L = \hat{L} - L$. $\langle \Delta L \rangle$ and $\sigma_{\Delta L}$, respectively, indicate the ensemble average and standard deviation. All values are in units of millimeters.

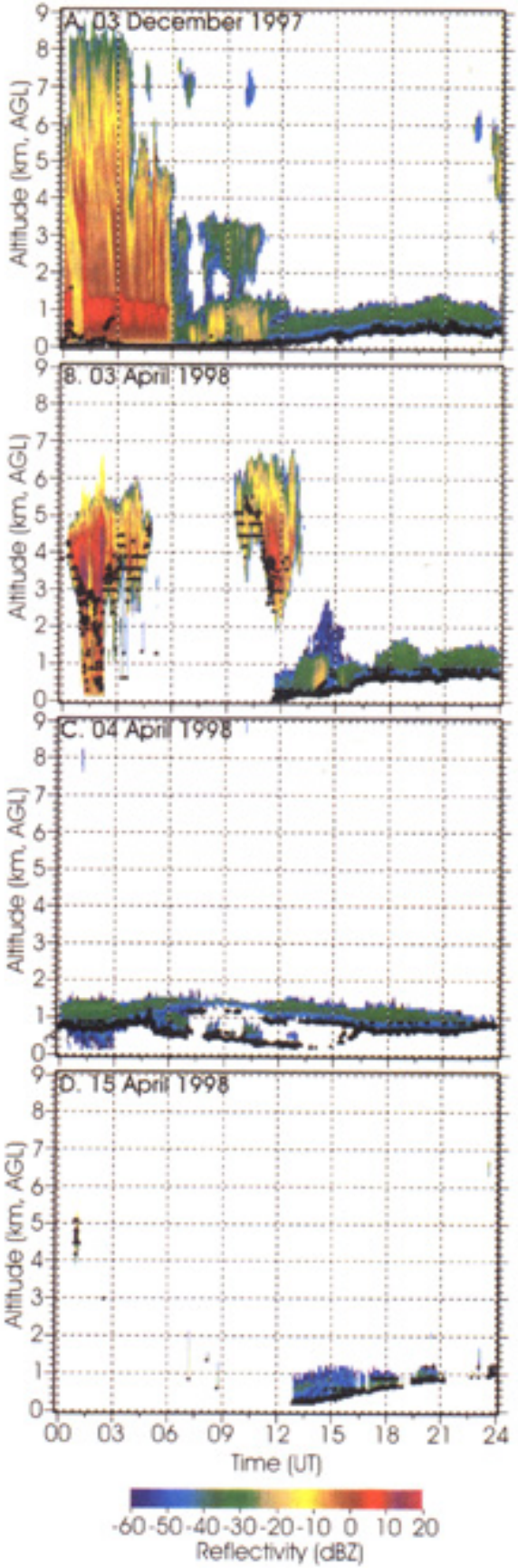

Plate 1. Millimeter-wave cloud radar reflectivities on the four case study days of (a) December 3, 1997, (b) April 3, 1998, (c) April 4, 1998, and (d) April 15, 1998. The black solid dots indicate the cloud base heights from a combined analysis of micropulse lidar and laser ceilometer data.

site (top), the values increase to 281 K and 0.040 mm, respectively. For each of these cases the median value of $\hat{L}$ is very close to zero.

The general trend of these distributions to exhibit negative values of $\hat{L}$ at the extreme values of T_{cloud} reflects the fact that the extreme values are outside the range used to develop estimators (17) for l_1 and l_2 (Figure 1). This situation is more pronounced for the tropical site than the polar sites because the PWV is much greater at the tropical site. At all sites, as T_{cloud} falls below the range of the values upon which $\hat{l}_1$ and $\hat{l}_2$ were based (i.e., as it falls below the range where liquid water clouds would be expected to exist), $\hat{L}$ is always negative. This observation provides a straightforward method for detecting "clear" (i.e., liquid free) sky conditions using the radar-derived estimate of T_{cloud}: if $\hat{L}$ is less than zero, then $\hat{L}$ is set equal to zero.

When the sky is truly cloud-free, the estimate of T_{cloud} is zero because the weighting function (16) derived from the radar reflectivity is zero, so $\hat{L}$ will always unambiguously indicate clear-sky conditions. Even high-altitude ice clouds, which are readily detectable by the radar, will not (normally) cause the new retrieval to produce positive values of $\hat{L}$, because the radar-derived values of T_{cloud} will (normally) be less than the value for which $\hat{L} > 0$. Thus thin clouds may be unambiguously distinguished from clear-sky conditions with the new site-independent retrieval, whereas the two are often indistiguishable with the current site-specific retrieval. However, mixed-phase clouds can be a problem if the radar reflectivity of the ice-phase particles is comparable to the reflectivity of the liquid phase. This situation would bias T_{cloud} low and result in an underestimate of L. In addition, drizzle below cloud base would tend to bias T_{cloud} high and result in an overestimate of L.

Accurate estimates of T_{cloud} are an important component of the new site-independent retrieval. However, if radar data are unavailable from which to produce estimates of T_{cloud} via (15) and (18), the new retrieval should nonetheless provide LWP estimates comparable in accuracy to estimates from the site-specific retrieval. The statistics in Table 4 reveal that the site-independent retrieval with coefficients l_1 and l_2 given by (19) yields results comparable to the site-specific retrieval, except that at larger values of L, a bias arises because of differences in the values of $\langle T_{\text{cloud}} \rangle$ inherent in the respective retrievals.

3.2. Comparison of LWP Retrievals on Four Case Study Days

To illustrate the performance of the new site-independent retrieval with actual data, we applied the retrieval to the brightness temperatures measured with a microwave radiometer at the ARM SGP central facility on December 3, 1997, and April 3, 4, and 15, 1998. These days were chosen because the millimeter-wave cloud radar (MMCR) indicated well-defined stratus clouds (Plate 1) and because each day exhibited a different range of retrieved LWP from the other days. Mea-

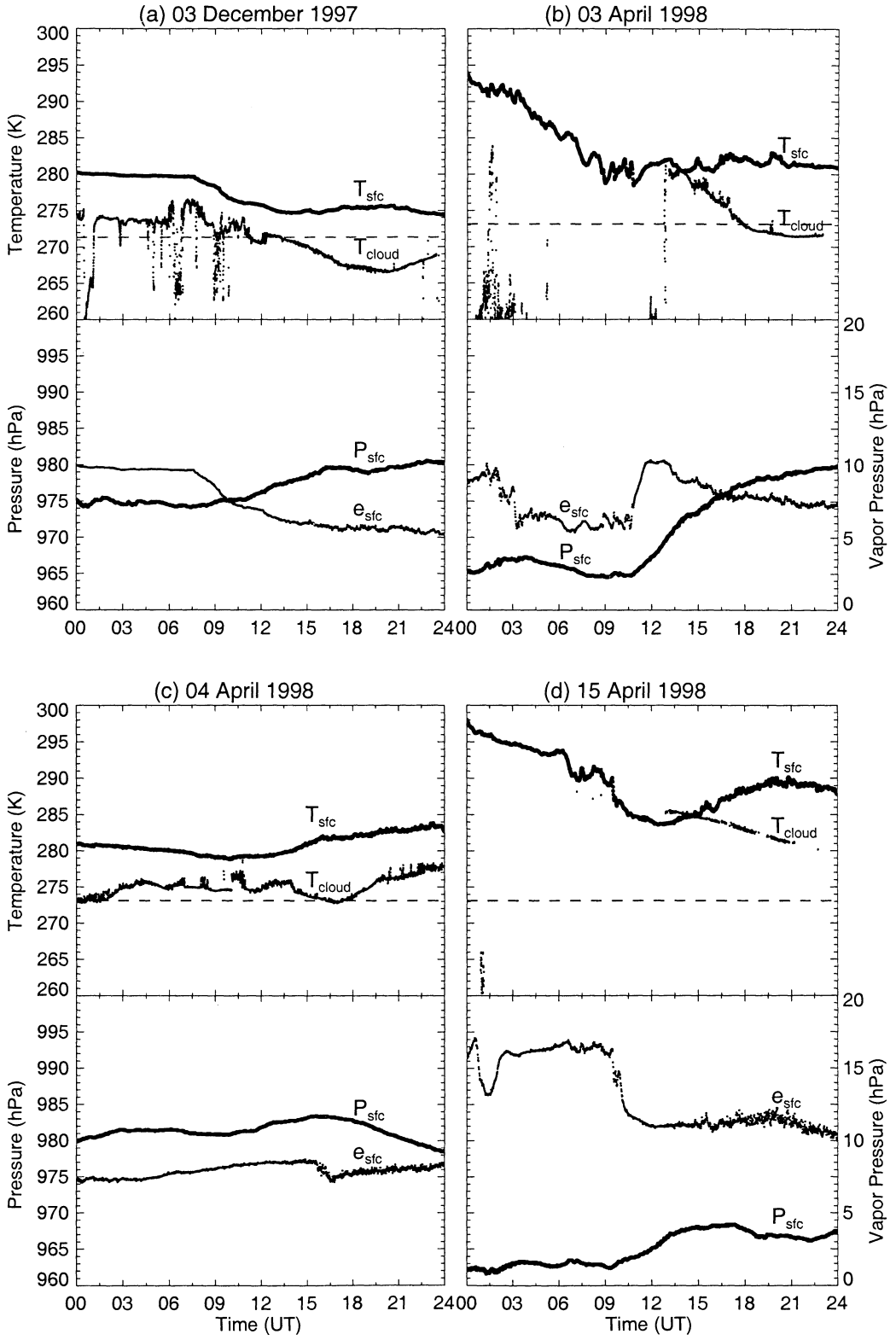

Figure 4. Surface temperature T_{sfc}, liquid water-weighted cloud temperature T_{cloud}, surface pressure P_{sfc}, and water vapor pressure e_{sfc}, for the four case study days of (a) December 3, 1997, (b) April 3, 1998, (c) April 4, 1998, and (d) April 15, 1998. The dashed line in the top plot for each day represents the value of $\langle T_{\mathrm{cloud}} \rangle$ for that month.

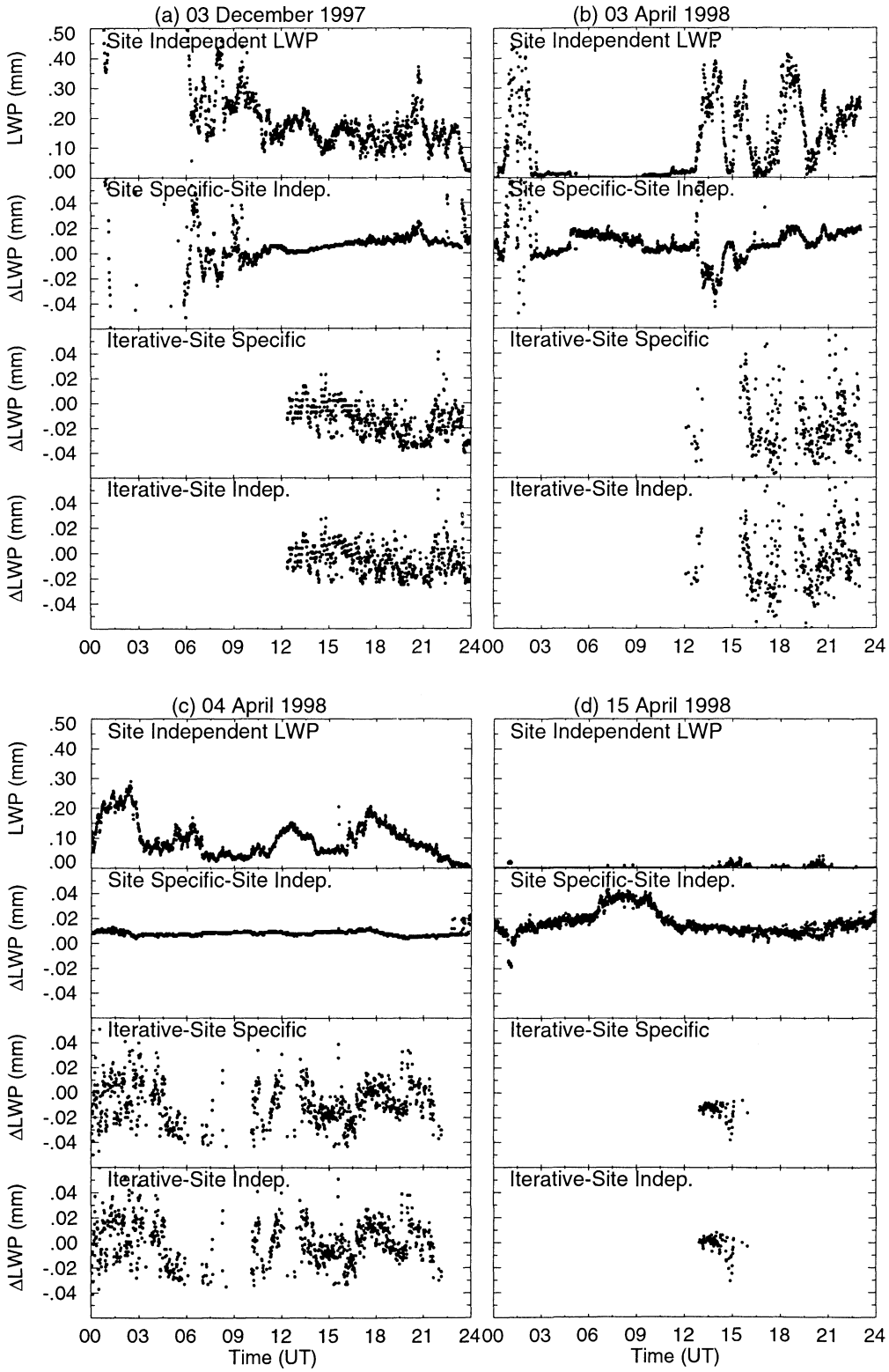

Figure 5. Liquid water paths (LWPs) from the new retrieval (top), with the differences in LWP between the site-specific and the new retrievals (second panel), the iterative and site-specific retrievals (third panel), and the iterative and new retrievals (bottom) for the four case study days of (a) December 3, 1997, (b) April 3, 1998, (c) April 4, 1998, and (d) April 15, 1998.

Table 5. Comparison of Site-Independent (SI), Site-Specific (SS), and Iterative (IT) Liquid Water Path Retrievals Over 4 Days

		SS - SI		IT - SS		IT - SI		IT
Day	Samples	$\langle \Delta L \rangle$	$\sigma_{\Delta L}$	$\langle \Delta L \rangle$	$\sigma_{\Delta L}$	$\langle \Delta L \rangle$	$\sigma_{\Delta L}$	RMSE
December 3, 1997	660	0.009	0.009	-0.013	0.013	-0.004	0.014	0.011
April 3, 1998	343	0.011	0.009	-0.016	0.027	-0.005	0.027	0.012
April 4, 1998	837	0.008	0.003	-0.007	0.017	0.001	0.018	0.014
April 15, 1998	42	0.011	0.002	-0.017	0.006	-0.006	0.007	0.000

$\Delta L = \hat{L} - L$. $\langle \Delta L \rangle$ and $\sigma_{\Delta L}$ indicate the ensemble average and standard deviation. All values are in units of millimeters.

surements of the surface pressure P_{sfc}, the surface vapor pressure e_{sfc}, the surface temperature T_{sfc}, and the mean cloud temperature T_{cloud} for these four days are in Figure 4.

The LWP retrievals over the four case study days exhibited trends expected from the results for the simulated radiometer measurements presented above. In particular, significant changes in T_{cloud} during a stratus event produced trends between the new site-independent and site-specific LWP retrievals. For retrieved LWPs that exceeded 0.25 mm, the site-specific retrieval underestimated LWP relative to the site-independent retrieval when $T_{\text{cloud}} > \langle T_{\text{cloud}} \rangle$ and overestimated LWP when $T_{\text{cloud}} \leq \langle T_{\text{cloud}} \rangle$. Importantly, the site-independent retrieval correctly identified the clear-sky periods in the partly cloudy conditions, whereas the nonzero values of LWP obtained with the site-specific retrieval during clear-sky periods were comparable in magnitude to LWP values retrieved during subsequent cloudy conditions.

Examples of trends in T_{cloud} leading to differences between the site-specific and site-independent retrievals occurred on December 3, 1997, and April 3, 1998. From 1200-1330 UT on December 3, 1997, T_{cloud} was approximately equal to the monthly climatological value of $\langle T_{\text{cloud}} \rangle = 271.35$ K (Figure 4a), and the two retrievals produced nearly identical results (Figure 5a). Over the following 6-hour period, T_{cloud} dropped by approximately 6 K, during which time the site-specific retrieval LWP values increased relative to the site-independent retrieval values. Such a bias in the site-specific retrieval is expected because the site-specific retrieval compensates for an overestimate in T_{cloud} by increasing the retrieved LWP.

From 1330-2230 UT on April 3, 1998, T_{cloud} dropped by approximately 8 K (Figure 4b). At 1800 UT, T_{cloud} fell from a level higher than the monthly value of $\langle T_{\text{cloud}} \rangle = 273.13$ K to a level lower than the monthly value. Before 1800 UT the site-specific retrieval tended to underestimate the LWP. In contrast, after 1800 UT the site-specific retrieval overestimated LWP, in keeping with the interpretation of Figure 2. Particularly noteworthy periods on April 3, 1998, are 1330-1400 UT, 1500-1630 UT, 1800-1930 UT, and 2030-2100 UT, when the retrieved LWPs exceeded 0.25 mm. During the first two periods, which occurred when $T_{\text{cloud}} > \langle T_{\text{cloud}} \rangle$, the site-specific retrieval underestimated the LWP. The later two time periods occurred when $T_{\text{cloud}} \leq \langle T_{\text{cloud}} \rangle$ and, in agreement with Figure 2, the site-specific retrieval overestimated the LWP. Between the pulses of large LWP the retrievals differ by no more than 0.005-0.010 mm over a 0.0 to 0.1 mm range of LWP values.

Problems in the site-specific retrievals during clear-sky periods are illustrated by the results for April 15, 1998 (Plate 1d, Figure 4d, and Figure 5d). At 0600-0900 UT on this day, the radar and lidar indicated clear sky, while at approximately 1300-2100 UT, both instruments detected a boundary layer stratus cloud. During both of these periods, the site-specific retrieval reported LWP values of 0.00-0.04 mm. Evidently, for the first period the site-specific retrieval responded to rapidly changing, cloud-free meteorological conditions, as reflected in the surface measurements (Figure 4d). For values of T_{cloud} derived by using the reflectivity profiles from the MMCR and the temperature profile from radiosondes, the new retrieval reports significant LWP values only during the second period.

The site-independent and site-specific retrievals showed the best agreement on April 4, 1998, differing by no more than approximately 0.01 mm throughout the day (Figure 5c). Near 0000 and 1630 UT, T_{cloud} equaled the monthly climatological value of $\langle T_{\text{cloud}} \rangle = 273.13$ K. However, the maximum difference between the two algorithms occurred at these times, clearly demonstrating a small bias between them on this day. When T_{cloud} increased by 3 K and 5 K just after 0200 UT and 1800 UT, respectively, the bias decreased to values comparable to those during the small-LWP periods at 1200-2400 UT on April 3, 1998 (Figures 5b and c).

The tendency of the site-specific retrieval to overestimate LWP relative to the site-independent retrieval is demonstrated further by the average difference between the two retrievals on each of the four case study days for times when the iterative retrieval reported a value (Table 5). On each day the iterative retrieval produced daily average LWP values less than the site-specific retrieval. Because the iterative retrieval was initialized with site-specific retrievals of PWV and LWP, the av-

erage effect of the iterative retrieval was to reduce the site-specific LWP. As Table 5 further indicates, the final LWP values produced by the iterative retrieval were even slightly less than the site-independent retrieval values. Using the iterative retrieval brightness temperature perturbation analysis described in section 2.4 as a surrogate for the total error in the iterative retrieval (including, for example, error produced by assuming that the radar reflectivity is an accurate predictor of liquid water content), we find that the RMS differences between the site-independent and iterative retrievals are comparable in magnitude to the errors expected in the iterative retrieval (Table 5).

4. Conclusions

We have developed new retrieval algorithms for cloud liquid water path and precipitable water vapor for use with microwave radiometric measurements by first identifying the physical processes that govern the microwave radiative transfer and then developing functional relationships to describe these processes using the atmospheric parameters that most affect them. By focusing on the underlying physics, our retrieval is more akin to functional approximation rather than the statistical estimation associated with standard statistical retrieval methods. Because of this approach, our retrieval is independent of the climatology of any particular site and may thus be applied to any location. Not only does this eliminate the need to develop retrievals for each measurement location but it also allows the retrieval to adapt to changing conditions at any given location. Importantly, the new site-independent precipitable water vapor retrieval is as accurate as a statistical retrieval developed specifically for a particular location (Appendix A).

Through the use of simulations and case studies, we have shown that accounting for the temperature dependence of the mass absorption coefficient for liquid water by including the liquid-water-weighted mean cloud temperature in the retrieval dramatically improves the accuracy of the liquid water path estimate relative to simpler statistical retrieval algorithms. Although we used a cloud radar to estimate the weighting function for the liquid-weighted-mean cloud temperature, the algorithm does not specifically require radar reflectivities, only a reasonable estimate of the liquid-weighted-mean cloud temperature.

Finally, by including liquid-weighted-mean cloud temperature and accounting for local variations in surface conditions, clear-sky biases in the liquid water path which are evident in simpler statistical retrievals, and have for so long vexed users of the liquid water path measurements, have now been largely eliminated with the new retrieval.

Appendix A: Precipitable Water Vapor Comparisons

To evaluate the skill of the new site-independent water vapor retrieval, opacities were calculated according to (9) by using mean radiating temperatures estimated from the surface parameters with (11) and the simulated radiometer brightness temperatures. The oxygen contributions were then estimated with (13) and subtracted. The adjusted opacities were used to produce estimates of the precipitable water vapor with the new retrieval coefficients (14). Differences, $\Delta V = \hat{V} - V$, between the retrieved precipitable water vapor $\hat{V}$ and the precipitable water vapor obtained by integrating the soundings, V, were then calculated (Table A1). Only cloudy soundings were used to develop the new vapor retrieval coefficients via (14), although both clear and cloudy soundings were used to develop the estimators for T_{mr} and τ_{dry}. Consequently, the clear-sky simulation results represent a semi-independent test of the algorithm. Comparison of the standard deviations in Table A1 with the medians of precipitable water vapor

Table A1. Comparison of Precipitable Water Vapor From Site-Independent and Site-Specific Retrievals Using Simulated Brightness Temperature Measurements

	Clear Sky				Cloudy Sky			
	Site-Independent Retrieval		Site-Specific Retrieval		Site-Independent Retrieval		Site-Specific Retrieval	
Site	$\langle\Delta V\rangle$	$\sigma_{\Delta V}$	$\langle\Delta V\rangle$	$\sigma_{\Delta V}$	$\langle\Delta V\rangle$	$\sigma_{\Delta V}$	$\langle\Delta V\rangle$	$\sigma_{\Delta V}$
SHEBA	0.05	0.32	0.08	0.29	-0.05	0.39	0.08	0.33
Barrow, Alaska	0.00	0.38	0.02	0.30	-0.12	0.39	0.02	0.32
Manus Is., Papua New Guinea	-0.01	0.42	0.02	0.38	0.03	0.54	-0.09	0.48
Morris, Oklahoma	-0.08	0.45	-0.18	0.42	-0.05	0.58	-0.31	0.55
Lamont, Oklahoma	0.08	0.43	0.05	0.39	0.03	0.54	-0.12	0.53
Purcell, Oklahoma	-0.02	0.44	0.07	0.39	-0.06	0.57	-0.12	0.54
Hillsboro, Kansas	0.01	0.43	0.16	0.38	0.00	0.50	0.03	0.49
Vici, Oklahoma	0.05	0.40	0.41	0.41	-0.10	0.51	0.22	0.49
Albuquerque, New Mexico	-0.04	0.29	0.00	0.31	-0.22	0.35	-0.04	0.36

$\Delta V = \hat{V} - V$. $\langle\Delta V\rangle$ and $\sigma_{\Delta V}$ indicate the ensemble average and standard deviation. All values are in units of millimeters.

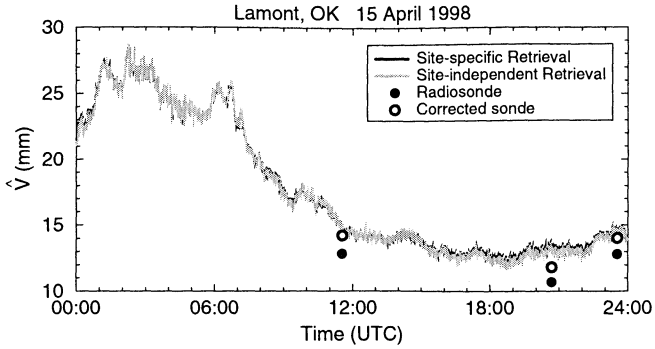

Figure A1. $\hat{V}$ derived by using the current site-specific statistical retrieval (black curve) and the new site-independent retrieval (gray curve) for the ARM central facility near Lamont, Oklahoma. The two retrievals give nearly identical results for this case. A comparison with standard radiosonde measurements (solid circles) and relative-humidity-corrected sondes (open circles) is also shown.

presented in Table 1 for corresponding sites suggests that the new retrieval, on average, is accurate to about 2-3%.

Differences between precipitable water vapor values estimated with the site-specific retrieval currently in use by ARM at each of these sites and the actual values from the soundings are also shown in Table A1. For each site, the new site-independent retrieval gives an unbiased estimate of V with a standard deviation comparable to that for the site-specific statistical retrieval. The bias in the current site-specific retrieval for Vici, Oklahoma, is significant. This bias arises because Vici is 660 m above sea level, whereas the site-specific retrieval was based on soundings from Oklahoma City, Oklahoma, about 300 m above sea level. This elevation difference corresponds to a difference in mean surface pressure of about 35 hPa (Table 1). Similarly, a negative bias arises at Morris, Oklahoma, which is only about 200 m above sea level. By accounting for the pressure dependence, the new site-independent retrieval eliminates these biases.

Apart from the biases at Vici and Morris, the two retrievals produced comparable values for PWV. For example, values of $\hat{V}$ for April 15, 1998, from the current site-specific and new site-independent retrievals are presented in Figure A1. For this day, which is typical of most days, the two retrievals yield essentially identical PWV results. In addition, $\hat{V}$ from both of the retrievals agrees reasonably well with radiosonde-derived PWV estimates after a correction developed by Vaisala was applied to the sonde relative humidity measurements.

Instrument errors contribute only about 20-25% to the total error in the retrieved PWV; that is, if no noise was added to the brightness temperatures to simulate an actual radiometer, the standard deviations of the differences would still be about 75-80% of the values presented in Table A1. Most of the error in $\hat{V}$ arises from errors in the estimators for T_{mr}, τ_{dry}, v_1, and v_2.

Acknowledgments. This research was supported by the Environmental Sciences Division of U.S. Department of Energy as part of the Atmospheric Radiation Measurement Program. James Liljegren was supported under contracts CHENG82-1010502-0002884 at Ames Laboratory, where much of this work was performed, and W-31-109-Eng-38 at Argonne National Laboratory. Eugene Clothiaux was supported under grant DE-FG02-90ER61071. Seiji Kato was supported by the National Aeronautics and Space Administration Clouds and the Earth's Radiant Energy System grant NAG-1-1963. Data were obtained from the Atmospheric Radiation Measurement (ARM) Program sponsored by the U.S. Department of Energy, Office of Science, Office of Biological and Environmental Research, Environmental Sciences Division. The authors thank Barry Lesht at Argonne National Laboratory for providing the relative-humidity-corrected radiosonde data and Marvin Wesely, also at Argonne, for carefully reviewing an early draft of the manuscript. The authors are grateful for the insightful comments and suggestions from the four anonymous reviewers, especially one reviewer who pointed out subtleties in the algorithm that we had not clearly highlighted.

References

Cahalan, R. F., and J. H. Joseph, Fractal statistics of cloud fields, *Mon. Weather Rev., 117,* 261-272, 1989.

Cahalan, R. F., W. Ridgeway, W. J. Wiscombe, T. L. Bell, and J. B. Snider, The albedo of fractal stratocumulus clouds, *J. Atmos. Sci., 51,* 2434-2455, 1994.

Cess, R. D., et al., Intercomparison and interpretation of climate feedback processes in 19 atmospheric general circulation models, *J. Geophys. Res., 95,* 16,601-16,615, 1990.

Committee on Earth and Environmental Sciences (CEES), *Our Changing Planet: The FY 1991 Research Plan of the U.S. Global Change Research Program,* U.S. Geol. Surv., Washington, D.C., 1990.

Davis, A., A. Marshak, W. Wiscombe, and R. Cahalan, Multifractal characterization of nonstationarity and intermittency in geophysical fields: Observed, retrieved, or simulated, *J. Geophys. Res., 99,* 8055-8072, 1994.

Decker, M. T., E. R. Westwater, and F. O. Guiraud, Experimental determination of ground-based microwave radiometric remote sensing of atmospheric temperature and water vapor profiles, *J. Appl. Meteorol., 17,* 1788-1795, 1978.

Frisch, A. S., G. Feingold, C. W. Fairall, T. Uttal, and J. B. Snider, On cloud radar and microwave radiometer measurements of stratus cloud liquid water profiles, *J. Geophys. Res., 103,* 23,195-23,197, 1998.

Ghan, S. J., L. R. Leung, and Q. Hu, Application of cloud microphysics to NCAR CCM, *J. Geophys. Res., 102,* 16,507-16,527, 1997.

Han, Y., and E. R. Westwater, Remote sensing of tropospheric water vapor and cloud liquid water by integrated ground-based sensors, *J. Atmos. Oceanic Technol., 12,* 1050-1059, 1995.

Liebe, H. J., and D. H. Layton, Millimeter-wave properties of the atmosphere: Laboratory studies and propagation modeling, *NTIA Rep. 87-224,* Natl. Telecom. and Inf. Admin., Boulder, Colo., 1987.

Liljegren, J. C., Two-channel microwave radiometer for observations of total column precipitable water vapor and cloud liquid water path, paper presented at the Fifth Symposium on Global Change Studies, Am. Meteorol. Soc., Nashville, Tenn., Jan. 23-28, 1994.

Rosenkranz, P. W., Absorption of microwaves by atmospheric gases, in *Atmospheric Remote Sensing by Microwave Radiometry,* edited by M. A. Janssen, pp. 37-90, John Wiley, New York, 1993.

Schroeder, J. A., and E. R. Westwater, User's guide to WPL microwave radiative transfer software, *NOAA Tech. Memo., ERL WPL-213*, NOAA ERL Wave Propagation Lab., Boulder, Colo., 1991.

Sheppard, B. E., Effect of rain on ground-based microwave radiometric measurements in the 20-90 GHz range, *J. Atmos. Oceanic. Technol., 13*, 1139-1151, 1996.

Stokes, G. M. and S. E. Schwartz, The Atmospheric Radiation Measurement (ARM) program: Programmatic background and the design of the clouds and radiation testbed, *Bull. Am. Meteorol. Soc., 75*, 1201-1221, 1994.

Westwater, E. R., Ground-based microwave remote sensing of meteorological variables, in *Atmospheric Remote Sensing by Microwave Radiometry*, edited by M. A. Janssen, pp. 145-213, John Wiley, New York, 1993.

Wielicki, B. A., R. D. Cess, M. D. King, D. A. Randall, and E. F. Harrison, Mission to planet Earth: Role of cloud and radiation in climate, *Bull. Am. Meteorol. Soc., 76*, 2125-2153, 1995.

E. E. Clothiaux, Department of Meteorology, The Pennsylvania State University, University Park, PA 16802. (e-mail: cloth@essc.psu.edu)

Xiquan Dong, Department of Meteorology, University of Utah, Salt Lake City, UT 84112. (e-mail: xdong@atmos.met.utah.edu)

Seiji Kato, NASA Langley Research Center, Mail Stop 420, 21 Langley Boulevard, Hampton, VA 23681-2199. (e-mail: kato@aerosol.larc.nasa.gov)

J. C. Liljegren, Argonne National Laboratory, Bldg. 203-ER 9700 South Cass Avenue, Argonne, IL 60439. (e-mail: liljegren@anl.gov)

G. G. Mace, Department of Meteorology, University of Utah, Salt Lake City, UT 84112. (e-mail: mace@atmos.met.utah.edu)

(Received June 13, 2000; revised November 8, 2000; accepted November 21, 2000.)